



Efficient synthesis of aligned nitrogen-doped carbon nanotubes in a fluidized-bed reactor

Jia-Qi Huang^a, Meng-Qiang Zhao^a, Qiang Zhang^{a,b}, Jing-Qi Nie^a, Li-De Yao^b, Dang Sheng Su^{b,c}, Fei Wei^{a,*}

^a Beijing Key Laboratory of Green Chemical Reaction Engineering and Technology, Department of Chemical Engineering, Tsinghua University, Beijing 100084, China

^b Department of Inorganic Chemistry, Fritz Haber Institute of the Max Planck Society, Faradayweg 4-6, D-14195 Berlin, Germany

^c Catalysis and Materials Division, Shenyang National Laboratory for Materials Science, Institute of Metal Research, Chinese Academy of Sciences, Shenyang 110016, China

ARTICLE INFO

Article history:

Received 19 April 2011

Received in revised form 8 October 2011

Accepted 25 October 2011

Available online 17 November 2011

Keywords:

Carbon nanotubes

Fluidized bed

Doped materials

Chemical vapor deposition

Nanotechnology

ABSTRACT

Vertically aligned nitrogen-doped carbon nanotubes (NCNTs) with uniform size distribution, large aspect ratio, good orientation, and high purity were employed as novel platforms to understand the dopant-induced perturbations and found widely applications in catalysis, electrochemistry, energy conversion and storages. However, the efficient way to synthesis CNTs with ordered alignment in large scale is still a challenge. We reported NCNTs were efficiently synthesized on a lamellar vermiculite catalyst in a fluidized-bed reactor. The catalysts and as-grown products can maintain good fluidization state during the whole growth process. The intercalated growth mode prevented the NCNT arrays from the disturbance of particle collisions in the fluidized bed. With the introduction of nitrogen precursor, N atoms were doped into CNTs and formed NCNTs with bamboo-like structure. The content of N doping can be tuned in a range of 1.55–4.23% and the distribution of N-containing functional groups can also be modified by changing either the growth temperatures or nitrogen sources (NH₃, 1,2-ethylenediamine, and pyridine). We explored the growth temperature ranging from 650 to 800 °C. High growth temperature led to a high NCNT yield (2.95 g_{NCNT}/g_{cat} h), large NCNT diameter (about 20 nm), and high graphitization degree. This provides a potential way for the controllable mass production of aligned NCNTs for applications in catalysis, materials science, energy conversion and storage, etc.

© 2011 Elsevier B.V. All rights reserved.

1. Introduction

The introduction of nitrogen as hetero-atoms into carbon nanotubes (CNTs) offers a possibility of tailoring their structural and electronic properties [1]. Nitrogen atoms doped within the graphene matrix act as electron donors and promote n-type conductivity. The nitrogen-doped CNTs (NCNTs) have metallic properties which are characterized by the presence of a donor state close to the Fermi level [2–4]. Thus, the NCNTs can be employed as novel platforms to understand the dopant-induced perturbations on physical properties of one-dimensional nanomaterials [1]. Recently, great interest has been paid on NCNTs for their potential applications in catalysis [5], energy conversion and storage [6], sensors [7], etc. For instance, NCNTs, as a kind of novel metal-free catalysts, can be used for oxygen reduction reaction [8], Knoevenagel condensation [9], and dehydration [10]. On the other hand, they serve as extraordinary supports for metal catalysts (such as Fe, Ru, Pt) for ammonia decomposition [11,12], oxygen reduction

[13,14], cinnamaldehyde hydrogenation [15], alcohols oxidation [16], H₂O₂ direct synthesis from H₂ and O₂ [17], and electrooxidation [18–21]. Also, the N atoms doped in CNTs can provide pseudo-capacitance for supercapacitor [22–25]. Vertically aligned NCNTs combine the advantages of the ordered alignment structure (such as uniform size distribution, large aspect ratio, good orientation, and high purity) with their pristine properties. Based on aligned NCNTs, advanced fuel cells [26], high current density field emission devices [27,28], advanced supercapacitor, and Li-ion batteries have been achieved. Furthermore, it is found that the properties of NCNTs were sensitive to the N doping content and the N-containing functional group distribution. Usually, high N-doping level provides more active sites for catalysis reaction and higher pseudo-capacitance [29]. For instance, the pyridinic-N site shows high activity for oxygen reduction reaction [30], and piperidine-N provides strong base site for catalysis [29]. Therefore, the large scale synthesis of the vertically aligned NCNTs in a controlled manner is one prerequisite for the potential industrial applications.

Entangled NCNTs were commonly grown on powder catalysts in a fixed bed reactor [31–34]. When some flat substrates (such as quartz plates and silicon wafers) were used in a

* Corresponding author.

E-mail address: wf-dce@tsinghua.edu.cn (F. Wei).

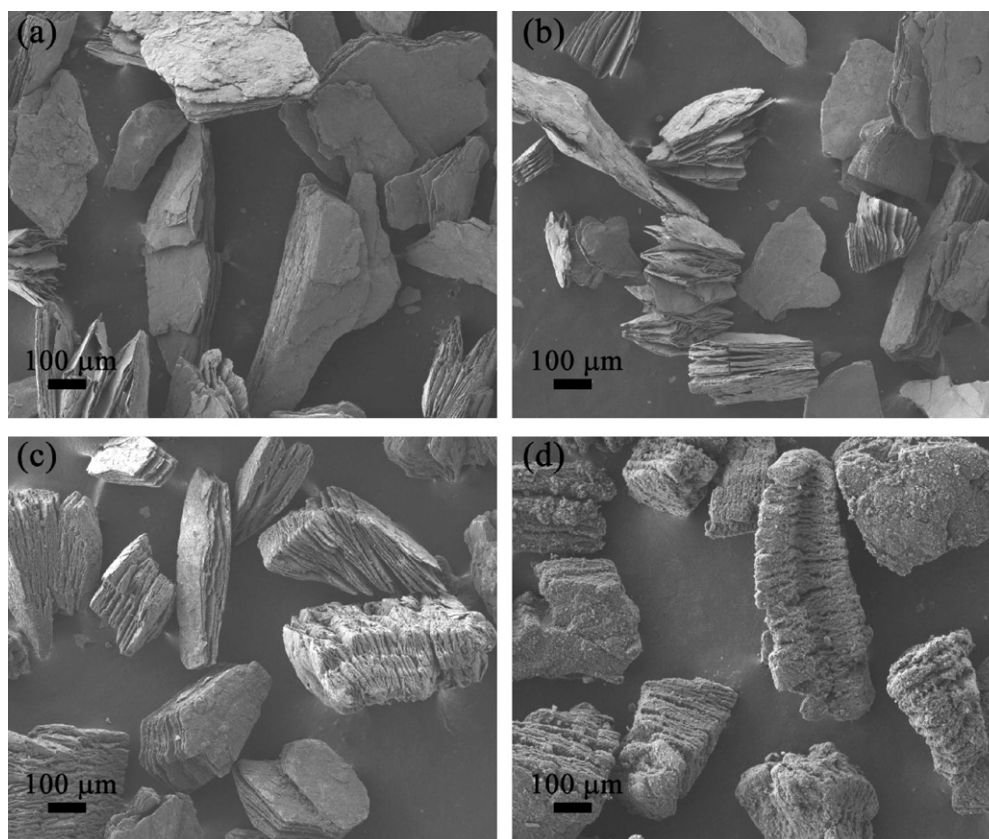


Fig. 1. Low magnification SEM images of (a) original vermiculite catalyst, and the products grown at (b) 650; (c) 700; (d) 800 °C.

chemical vapor deposition (CVD) reactor, NCNTs were synchronously synthesized with good alignment [14,35–38]. As the low surface area of flat substrates, the available area for aligned NCNT growth was therefore quite limited. The amount of the aligned CNTs is proportional to the surface area of a substrate. Thus, only milligram scale aligned CNTs can be synthesized for most batch-CVD growth. Although the fixed bed was widely used nowadays for the fabrication of the aligned NCNTs in laboratory, it suffered several engineering problems in scaling up, such as jam, non-uniform products in a same reactor, and low synthesis efficiency.

Up to now, CNTs have been mass produced on fluidizable catalysts in a fluidized bed reactor, benefiting from enough growth space, excellent diffusion and heat transfer, easiness in scaling up, and continuous operation [39–45]. Developing a fluidizable catalyst for aligned CNT growth is still a key issue. If the CNTs can be synthesized within an individual particle, then the collisions among CNT arrays during growth can be avoided. Based on this idea, we recently developed a fluidizable aligned CNT catalyst with natural lamellar metal phases among the inorganic layers as active metal phases [46]. Aligned CNTs were intercalatedly grown among the clay layers, thus, CNT product kept good alignments [47]. Mass production of aligned CNTs at a yield of 3.0 kg/h in a pilot-plant fluidized bed reactor was realized [48].

In this contribution, a route to synthesize vertically aligned NCNTs on lamellar catalyst in a fluidized bed reactor was reported by introducing nitrogen sources (such as NH_3 , 1,2-ethylenediamine, or pyridine) into the reactor. The N-doping level and the relative N-containing functional group amount can be tuned by the growth parameters. This provides a potential way for the controllable mass production of aligned NCNTs.

2. Experimental

2.1. Catalyst preparation

Vermiculite, a clay mineral which is a group of micaceous hydrated silicate minerals related to the chlorites and used in heat-expanded form as insulation and as a planting medium, was used as the catalyst support. The vermiculite used in our experiment was mined in Lingshou, Hebei Province of China. In brief, vermiculite particles with a size of 100–250 μm (bulk density of about 160 kg/m^3) were suspended in distilled water to form a uniform suspension through strong stirring at 80 °C. Subsequently, an aqueous solution of iron nitrate ($\text{Fe}(\text{NO}_3)_3 \cdot 9\text{H}_2\text{O}$) and ammonium molybdate ($(\text{NH}_4)_6\text{Mo}_7\text{O}_{24} \cdot 4\text{H}_2\text{O}$) was mixed with the suspension quickly. The mass ratio between vermiculite, water, iron nitrate, and ammonium molybdate was 20:100:5:1. The obtained mixture was kept at 80 °C for 5 h. After filtration, the filtrated cake was dried at 110 °C for 12 h and further calcined at 400 °C for 1 h using Ar/H_2 mixture gas (200 and 100 sccm) in a quartz tube (inner diameter 30 mm). Then the lamellar Fe/Mo/vermiculite catalyst for the production of aligned NCNTs was obtained. The minimal fluidization velocity (u_{mf}) of the lamellar catalyst was 1.6 cm/s. The catalysts were in fluidized state when the gas velocity was over u_{mf} . With an increasing gas velocity, several flow patterns or regimes identified as particulate fluidization, bubbling fluidization, turbulent fluidization, fast fluidization, and the pneumatic conveying regimes were achieved. The detailed fluidization behavior of this catalyst can be found in Ref. [47].

2.2. Aligned NCNT synthesis

For the synthesis of aligned NCNTs, NH_3 was used as the nitrogen source in a fluidized bed reactor with an inner diameter of

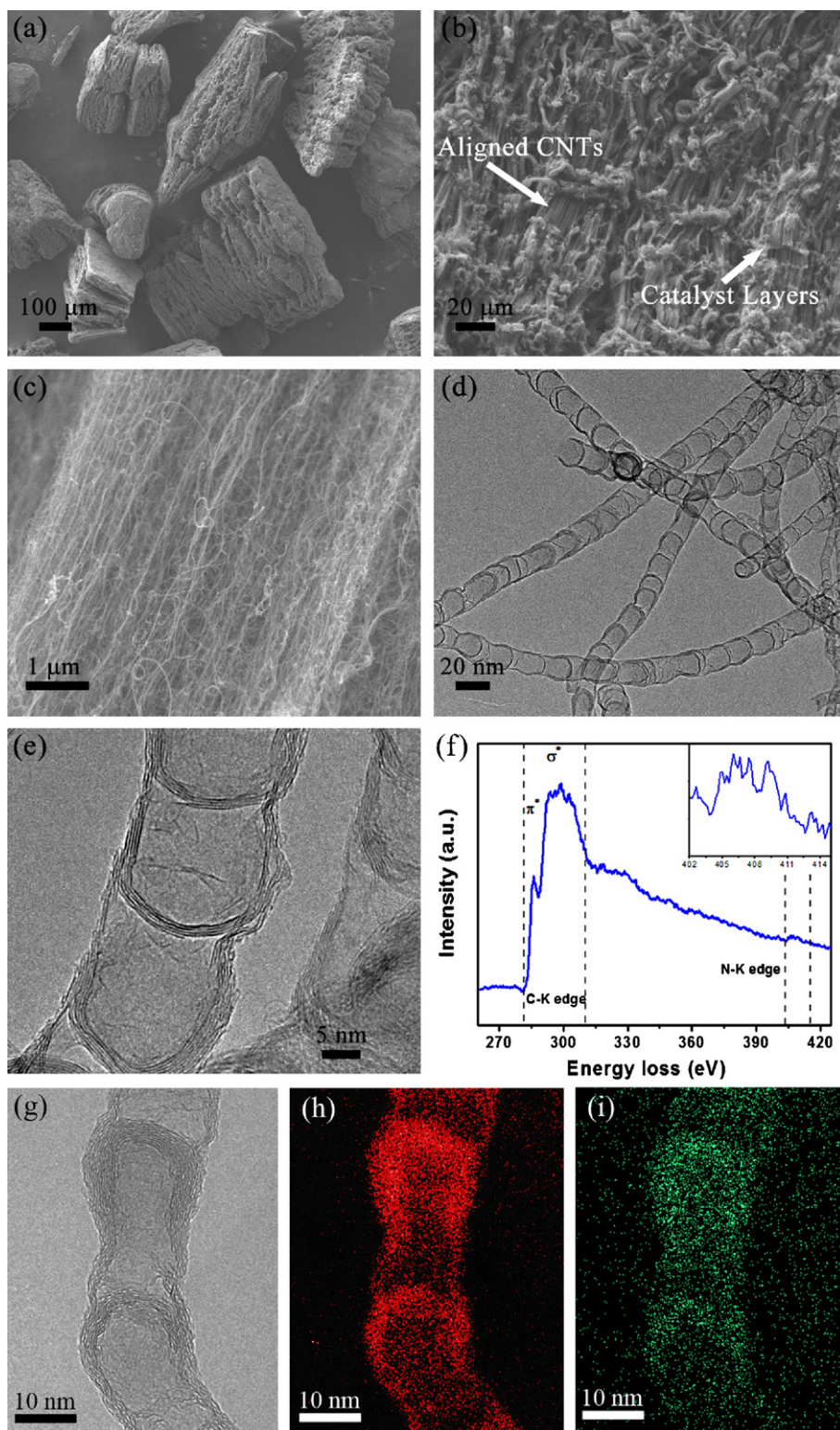


Fig. 2. (a and b) Low magnification SEM images of as-obtained products after CNT growth with NH_3 as nitrogen source at 750°C ; (c) high magnification SEM image showing the aligned NCNTs distributed between catalyst layers; (d) low and (e) high magnification TEM images of the as-prepared NCNTs; (f) EELS of the NCNTs; the insert is the enlarged spectrum of N-K edge; (g) high resolution TEM and (h–i) EFTEM image of NCNTs, where the red color stands for carbon, and the cyanine color stands for nitrogen. (For interpretation of the references to color in this figure legend, the reader is referred to the web version of the article.)

20 mm, and the lamellar Fe/Mo/vermiculite was selected as catalyst. About 1.0 g catalyst was fed into the reactor before reaction. The quartz fluidized bed reactor was then heated to reaction temperature in Ar atmosphere. After the reduction with H_2 , a mixture of $\text{C}_2\text{H}_4/\text{NH}_3/\text{H}_2$ was introduced into the fluidized bed and the

reaction occurred within the vermiculite particles. The catalysts were smoothly fluidized in the reactor, and the growth maintained for 30 min. After the reaction, the fluidized bed reactor cooled down under Ar atmosphere. The as-grown product was collected for further characterizations. Typical flow rates for Ar, H_2 , C_2H_4 ,

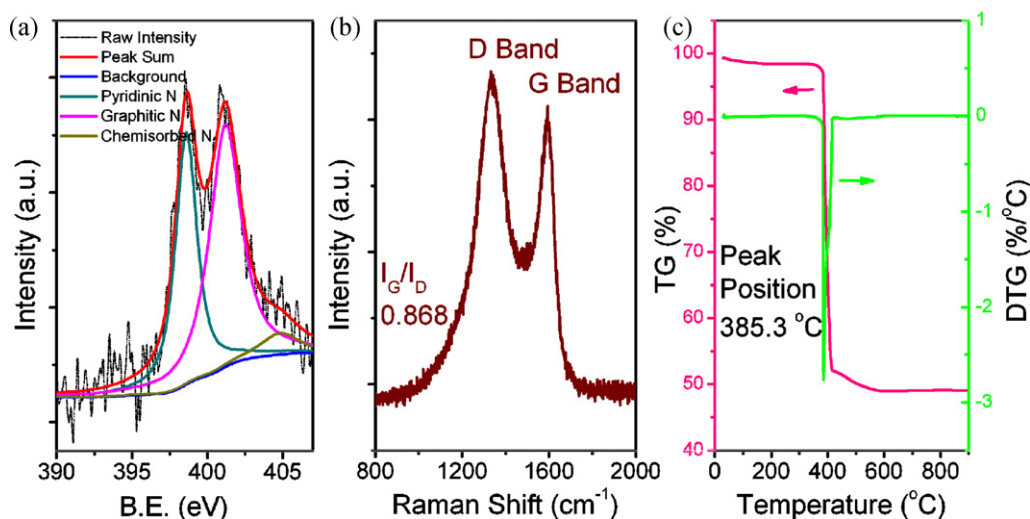


Fig. 3. (a) XPS narrow spectra in N region; (b) Raman spectra; (c) thermogravimetric (TG) and differential thermogravimetric (DTG) curves for aligned NCNTs with NH_3 as nitrogen source at 750°C .

and NH_3 were 200, 100, 100, and 60 sccm, respectively. The growth temperatures were in the range of $650\text{--}800^\circ\text{C}$. The gas velocity stood at about $7.5\text{--}8.7\text{ cm/s}$ under different growth temperatures, which kept both the catalysts and the as-produced products in stable fluidization state. We also synthesized un-doped CNTs for comparison with the exactly same condition except that no NH_3 was introduced. The synthesis of aligned NCNTs using pyridine or 1,2-ethylenediamine as nitrogen sources were in the similar conditions, except an additional vaporization process before entering the fluidized bed. Typical flow rates for Ar and H_2 were 200 and 100 sccm, respectively. The injection rates of liquid pyridine or 1,2-ethylenediamine were 10 or 11 mL/h, respectively.

2.3. Characterizations

The morphology of the aligned NCNTs was characterized using a JSM 7401F scanning electron microscope (SEM) operated at 5.0 kV, and a JEM 2010 high-resolution transmission electron microscope (TEM) operated at 120.0 kV. The specimens for TEM observation were prepared using a common sonication method. Raman experiments were performed with a Renishaw RM2000 Raman spectrophotometer. The spectra were recorded using a He–Ne laser excitation line at 632.8 nm on the aligned NCNTs at ambient temperature. The purity of NCNTs in the as-grown product was obtained through thermogravimetric analysis (TGA) by Mettler Toledo TGA/DSC-1, with a temperature ramp rate of $20^\circ\text{C}/\text{min}$ from 30 to 900°C . X-ray photoelectron spectroscopy (XPS) was used to determine the content of N element and the composition of N-containing functional groups with PHI Quantera SXM. The microstructures and energy filtered transmission electron microscopy (EFTEM) analysis of products were carried out on a Philips CM200 FEG TEM equipped with an image energy filter (GIF200, Gatan) at 200 kV. Electron energy-loss spectra (EELS) were acquired in diffraction mode at 0.1 eV per channel with a probe size of around 100 nm radius, circular region.

3. Results and discussion

3.1. Growth of aligned NCNTs in a fluidized bed

Lamellar vermiculite with intercalated Fe/Mo phase as the active composition was employed as the catalyst for the aligned NCNT synthesis. The pristine density of the vermiculite

catalyst is 2300 kg/m^3 , while the bulk density of the as-obtained Fe/Mo/vermiculite catalyst was just 160 kg/m^3 . According to the density and size distribution, the Fe/Mo/vermiculite catalyst particles belong to A particles according to Geldart particles classification [49]. Fig. 1a–d shows the low magnification SEM images of the catalyst before reaction, and the products by CVD growth at 650 , 700 , and 800°C , respectively. The original catalyst possessed a plate-like morphology with layer-stacked structure. With the intercalated growth of aligned NCNTs between the layers, the thickness of the catalyst increased. A vertically aligned CNT intercalated compound with a stick-like morphology was obtained. Though the size of the particles increased with the growth of aligned CNTs during the CVD growth, the powders can still maintain their fluidization status during the whole growth process.

The CNT growth with NH_3 as the nitrogen source was investigated as a typical process. Fig. 2a showed a low magnification SEM image of catalyst particles after half-hour growth. The catalyst particles turned into a worm-like structure with aligned CNTs intercalatedly distributed between the inorganic layers. Detailed observation showed that the intercalated CNT arrays were with a length of *ca.* $20\ \mu\text{m}$ (Fig. 2b, aligned NCNTs and catalyst layers were indicated by white arrows). With continuous growth of aligned NCNTs, the stress among the layers of vermiculite and arrays increased, leading to the breakage of the vermiculite layers. However, the as-grown NCNTs were still with good alignment in the direction perpendicular to the catalyst layers (Fig. 2c). Therefore, the as-obtained product was with alternate inorganic layers and aligned NCNTs. Fig. 2d and e illustrated the TEM images of the obtained NCNTs. The doping of N atoms altered the graphene structure of the multi-walled CNTs and led to a bamboo-like structure. This is quite different from un-doped CNTs with hollow inner core [43,46–48]. It was proposed that the carbon/nitrogen source decomposed and dissolved in the metal particles at high temperature. The migration of C/N atoms on the surface was the dominant process than diffusion through the catalyst nanoparticles. As a result, the N-doped graphene sheets precipitated from the catalyst particle and periodically pushed themselves out, which caused the formation of bamboo-like structures [34]. Here, the NCNTs were with large outer diameter (about 15 nm) and thin side walls (less than 10 walls). The side walls formed cap-like structure and stacked in the same direction to form the bamboo-like NCNTs. The inner hollow core was separated by the graphene layers into non-uniform compartments (length of $10\text{--}20\text{ nm}$). Unlike the un-doped

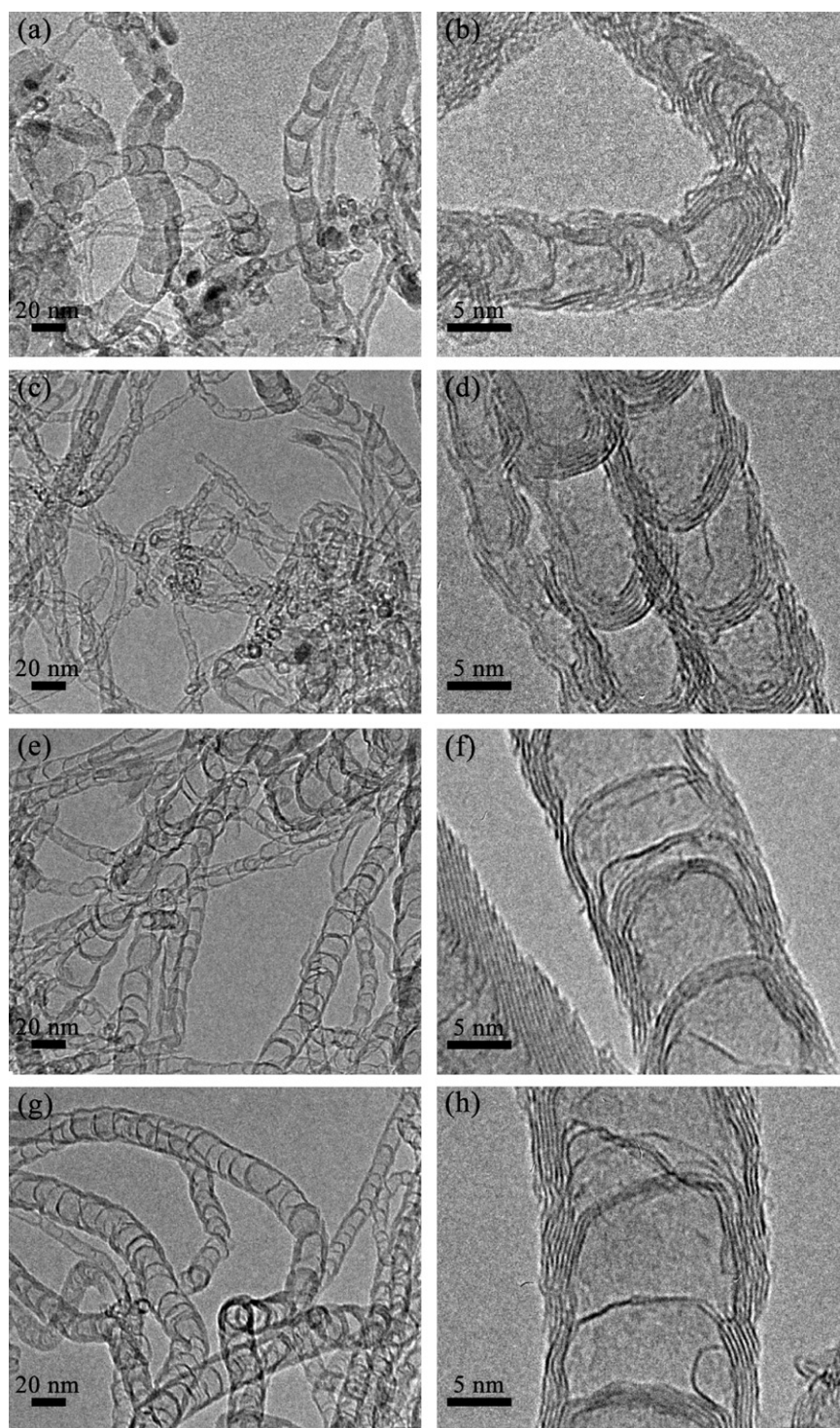


Fig. 4. Low and high magnification TEM images of NCNTs obtained at different growth temperatures: (a and b) 650 °C; (c and d) 700 °C; (e and f) 750 °C; (g and h) 800 °C.

CNTs with uniform side walls, the thicknesses of the side walls differed a lot. EELS measurement of the sample was presented in Fig. 2f. It was obtained from a circular region with 100 nm diameter including a couple of NCNTs perpendicular to the electron beam. Usually core-edge features in EELS occur when a core electron is promoted to an unoccupied state above the Fermi level. The EELS reveals the atomic environment, local electronic state as well as the doping level in CNTs. In the case of C–K edge, in-depth analysis of near-edge fine structure confirms the sp^2 -hybridized state of carbon, where the sharp 285.2 eV peak is due to the transition from

C 1s core level to π^* band. A broad band at about 293.3–310.2 eV corresponds to the transition to π^* orbital merged to the broad σ^* band. To estimate the relative sp^2 hybridization ratio, it is assumed that the ratio of integrated areas under π^* and σ^* peaks is proportional to the ratio of π and σ states [50]. And the sp^2 hybridization ratio was calculated as 0.17. Except for C–K edge, the N–K edge in Fig. 2f was also visible at around 403 eV, which confirmed the presence of nitrogen in CNTs. Fig. 2g–i presented the high resolution TEM and EFTEM images of the NCNTs, showing the element distribution of sample. The compartments of the NCNTs were clearly

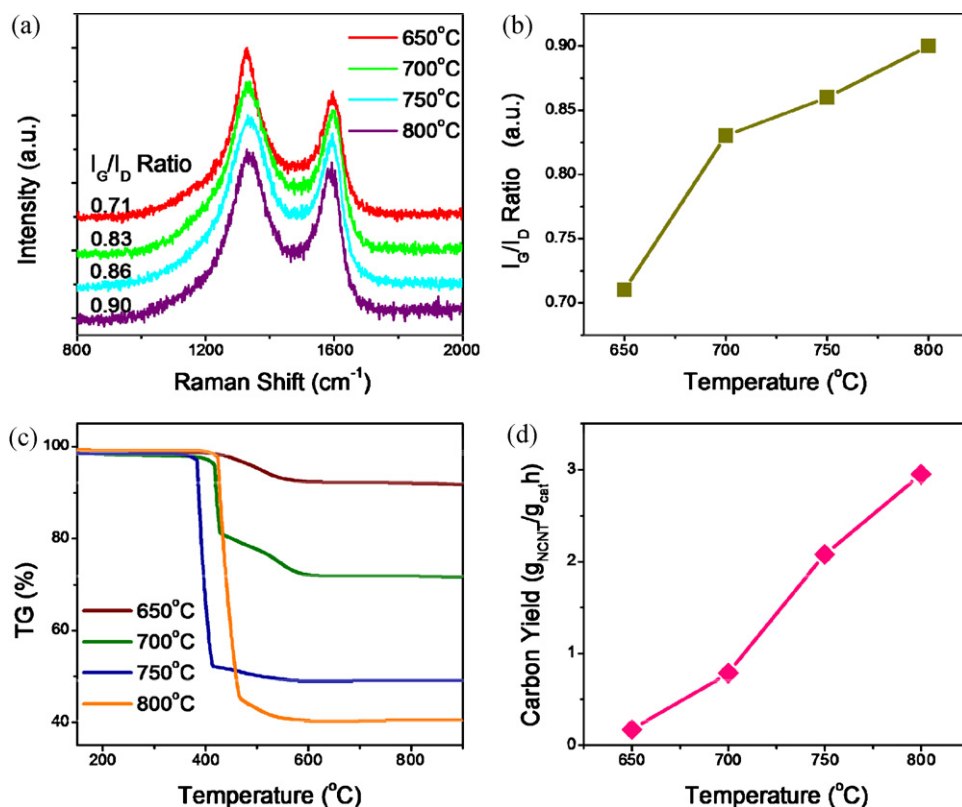


Fig. 5. (a) The Raman spectra and (b) the trend of I_G/I_D ratios for NCNTs grown under different temperatures; (c) the TG curves; (d) yields of NCNTs grown under different growth temperatures.

illustrated on the EFTEM images, showing that the N element was distributed almost homogeneously.

To determine the content and the relative ratio of different N-functional groups, XPS were employed and the N content of 4.23%

was determined. Fig. 3a showed the fine scan and gave clear evidence on the existence for N-containing functional groups. The N atoms in various N-containing functional groups exhibited different bonding environments and electronic structures, thus, different

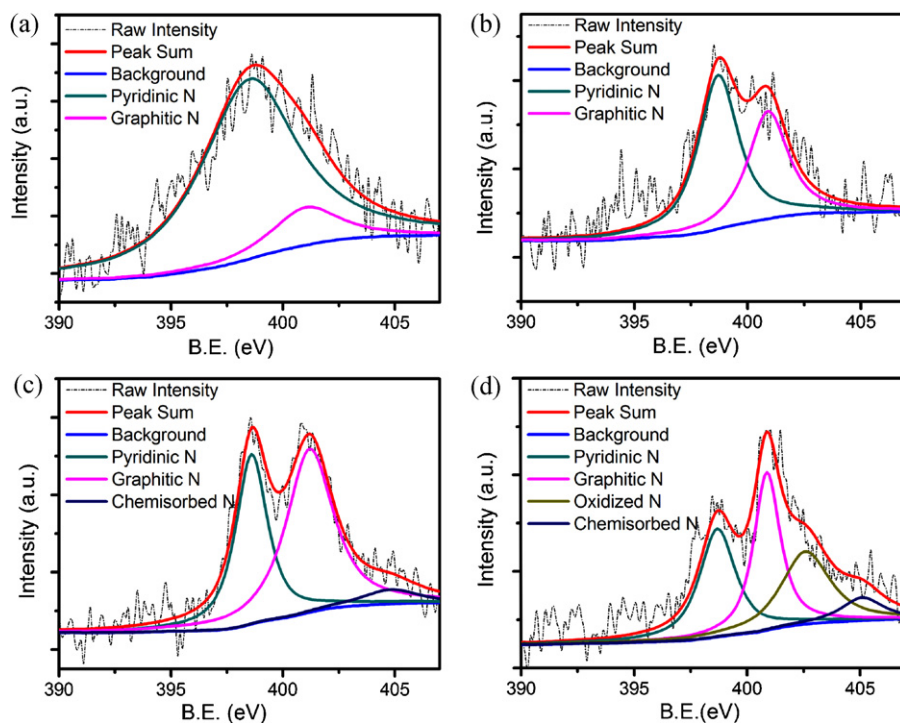


Fig. 6. XPS narrow spectra in N region of NCNTs produced using NH₃ as nitrogen source in fluidized bed at (a) 650; (b) 700; (c) 750; (d) 800 °C.

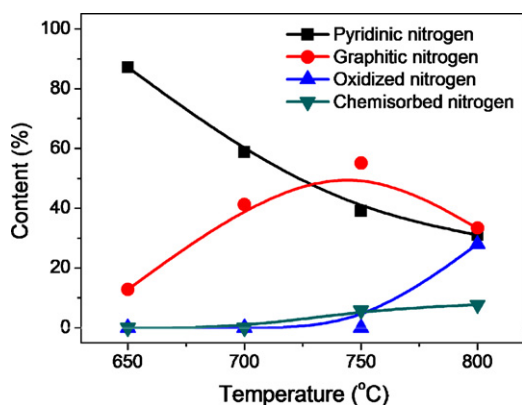


Fig. 7. The relative contents of N-containing functionalized groups in the aligned NCNTs synthesized under different growth temperatures.

peak positions appeared in the fine scan of XPS. The pyridinic N, pyrrolic N, graphitic N (coordinated N atoms substituting inner C atoms in the graphene layers), oxidized N, and chemisorbed N oxide were with corresponded binding energy peak positions at around 398.8, 400.0, 400.9, 403.0, and 405.2 eV, respectively [14]. The doped N atoms in this sample were mainly existed as pyridinic N, graphitic N, and chemisorbed N. The relative amount of N-containing functional groups can be estimated accordingly to be 39.1, 55.1, and 5.8%, respectively. Raman spectra were also used to identify the graphitization degree of the NCNTs (Fig. 3b). The intensity ratio of G peak (around 1580 cm^{-1} , assigned to the response of ordered graphite carbon structure) to D peak (around 1350 cm^{-1} , assigned to the response of disordered carbon structure) was determined to be 0.87, indicating a low graphitization degree of the NCNTs compared with the un-doped ones (0.94). This decline of I_G/I_D can be attributed to the doping of N atoms, which can replace the C atoms and resulted in the formation of non-hexagonal rings. The TGA curve (Fig. 3c) showed a sharp mass decrease to 49.1% at around $385\text{ }^\circ\text{C}$, the peak position was much lower than the un-doped CNTs at around $680\text{ }^\circ\text{C}$. This indicated that the introduction of N atoms to CNTs degraded their thermal stability and induced their oxidation at low temperature. The NCNT yield was $2.01\text{ g}_{\text{NCNT}}/\text{g}_{\text{cat h}}$ when the CVD growth was carried out at $750\text{ }^\circ\text{C}$.

3.2. Influence of growth temperature on aligned NCNT growth with NH_3 as nitrogen source

The synthesis of aligned NCNTs with NH_3 as nitrogen source was conducted at different growth temperatures (650, 700, 750 and $800\text{ }^\circ\text{C}$). Fig. 4 presented the low and high magnification TEM images of the NCNTs, displaying bamboo-like CNT structure and similar wall number of less than 10. However, the diameter of NCNTs increased from 5 to 20 nm when the growth temperature rose from 650 to $800\text{ }^\circ\text{C}$. The metallic nano-particles on the clay layers were prone to sinter into large ones at high temperature [48]. Thus, the obtained NCNTs were with larger inner and outer diameter accordingly. Unlike the un-doped CNTs, the NCNTs obtained under different growth temperatures demonstrated similar side wall numbers. This can be attributed to the fact that the metallic nanoparticles became unstable in the continuous precipitation of graphene layers. The fluctuation of C and N atoms caused the periodic formation of N-doped graphene layers mainly through the surface diffusion rather than bulk diffusion. Moreover, the formation of bamboo compartment would meet smaller stress in this situation [51].

The as-obtained NCNTs showed a higher I_G/I_D ratio with increasing growth temperature (Fig. 5a and b), which indicated that the higher growth temperature was helpful in improving of the

graphitization degree of the CNTs. Additionally, more NCNTs can be synthesized by increasing the growth temperature, which caused the as-grown products with larger particle size (Fig. 1). This was also verified by TGA results in Fig. 5c, where the carbon contents increased monotonically with the growth temperatures. With the increasing growth temperature from 650 to $800\text{ }^\circ\text{C}$, the carbon yield increased from 0.17 to $2.95\text{ g}_{\text{NCNT}}/\text{g}_{\text{cat h}}$ (Fig. 5d).

Based on XPS examinations, the N contents were estimated to be 2.03, 2.20, 4.23, and 2.41% for the growth temperatures from 650, 700, 750, and $800\text{ }^\circ\text{C}$, respectively. The fine scan (Fig. 6a–d) provided the information about the state of N-containing functional groups. The four samples included different kinds of N-containing functional groups, and the composition was rather complex for each sample obtained at high growth temperature. The pyridinic N can be found in all of the four samples. The pyridinic N can be formed at relatively low temperature and is generally accepted as one of the main reasons for the formation of bamboo-like structure. The doping of nitrogen as pyridinic N site is responsible for the curvature of graphitic walls, leading to the formation of wall roughness and also interlinked bamboo-like structure [52]. Graphitic N, which was the substituted N atom in a C hexatomic ring, was also found in all samples. When the NCNTs were synthesized at even higher temperature, the oxidized pyridinic N group and chemisorbed N group can be detected as well. Based on the peak area, the relative amounts of the N-containing functional groups in the products grown at different growth temperatures were estimated. As observed in Fig. 7, the ratios of four main functional groups change with the growth temperature. The ratio of pyridinic N decreased solely with the growth temperature from 87 to 30%, which was consistent with the reported behavior of pyridinic N under high temperature [53,54]. The substitution of N atoms for C atoms occurred at high temperature and the graphitic N reached a highest ratio of 55%. The oxidized N and chemisorbed N only appeared under high growth temperature, and the amount of oxidized N can reach 28% under $800\text{ }^\circ\text{C}$.

3.3. Influence of nitrogen source on aligned NCNT growth

Other nitrogen sources, such as 1,2-ethylenediamine and pyridine, were also used for the NCNT growth in the fluidized bed reactor. In fact, they can serve both as nitrogen and carbon sources during CVD growth. Fig. 8a and b showed the SEM images for the NCNTs from 1,2-ethylenediamine synthesized at $750\text{ }^\circ\text{C}$. Similar intercalated growth behavior can be observed. The NCNTs had a broad diameter distribution (Fig. 8b). The TEM images (Fig. 8c and d) verified the bamboo-like structure with the wall numbers varying from 5 to 15, which was with a wider distribution compared with NCNTs obtained using NH_3 as nitrogen source. Fig. 8e–g confirmed the doping of nitrogen into the CNT structure, and the nitrogen also distributed homogenous on the nanotube.

XPS characterization showed that the N content for NCNTs derived from 1,2-ethylenediamine was about 1.55% (Fig. 9a). The most N atoms stayed as graphitic N (64.0%). Small amount of pyridinic N (28.5%) and oxidized N (7.5%) were also detected. The as-grown sample was also with a similar I_G/I_D ratio compared with that obtained with NH_3 as nitrogen source (Fig. 9b). From the TGA curve, the position of weight loss peak was at $482\text{ }^\circ\text{C}$, and a NCNT yield of $1.30\text{ g}_{\text{NCNT}}/\text{g}_{\text{cat h}}$ was obtained (Fig. 9c).

When pyridine was used as both the carbon and nitrogen sources, the NCNTs showed alternate aligned NCNTs and inorganic layer morphology (Fig. 10a and b). The as-grown NCNTs illustrated a fishbone-like structure with an angle of $5\text{--}10^\circ$ between the graphene sheets and the tube axis. Besides, the side wall number was estimated to be around 13 (Fig. 10c and d), which was much larger than that obtained with NH_3 or 1,2-ethylenediamine as nitrogen source (Figs. 2e, 4 and 8d). The NCNTs derived from

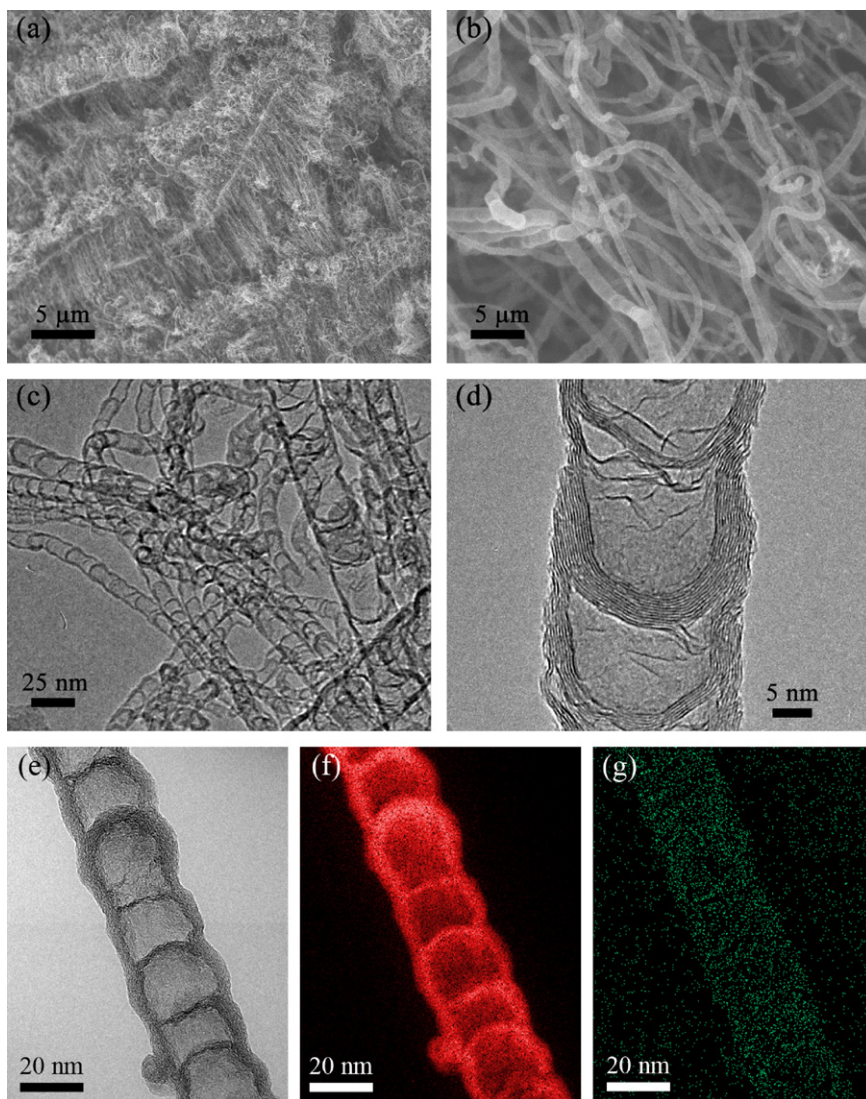


Fig. 8. (a) Low magnification and (b) high magnification SEM images; (c) low magnification and (d) high magnification TEM images of the aligned NCNTs grown at 750 °C with 1,2-ethylenediamine as nitrogen source; (e) the high resolution TEM and (f–g) the EFTEM images of NCNT, where the red color stands for carbon, and the cyanine color stands for nitrogen. (For interpretation of the references to color in this figure legend, the reader is referred to the web version of the article.)

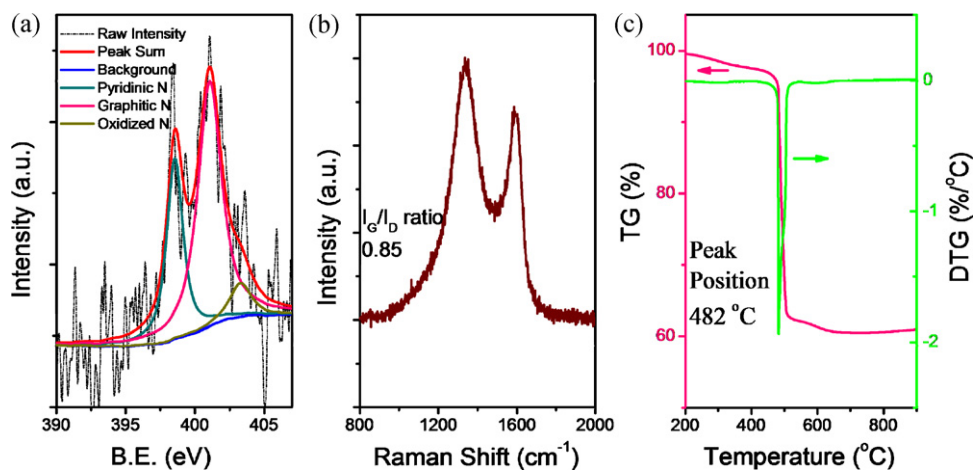


Fig. 9. (a) XPS narrow spectra in N region; (b) Raman spectra; (c) TG and DTG curves for aligned NCNTs with 1,2-ethylenediamine as nitrogen source at 750 °C.

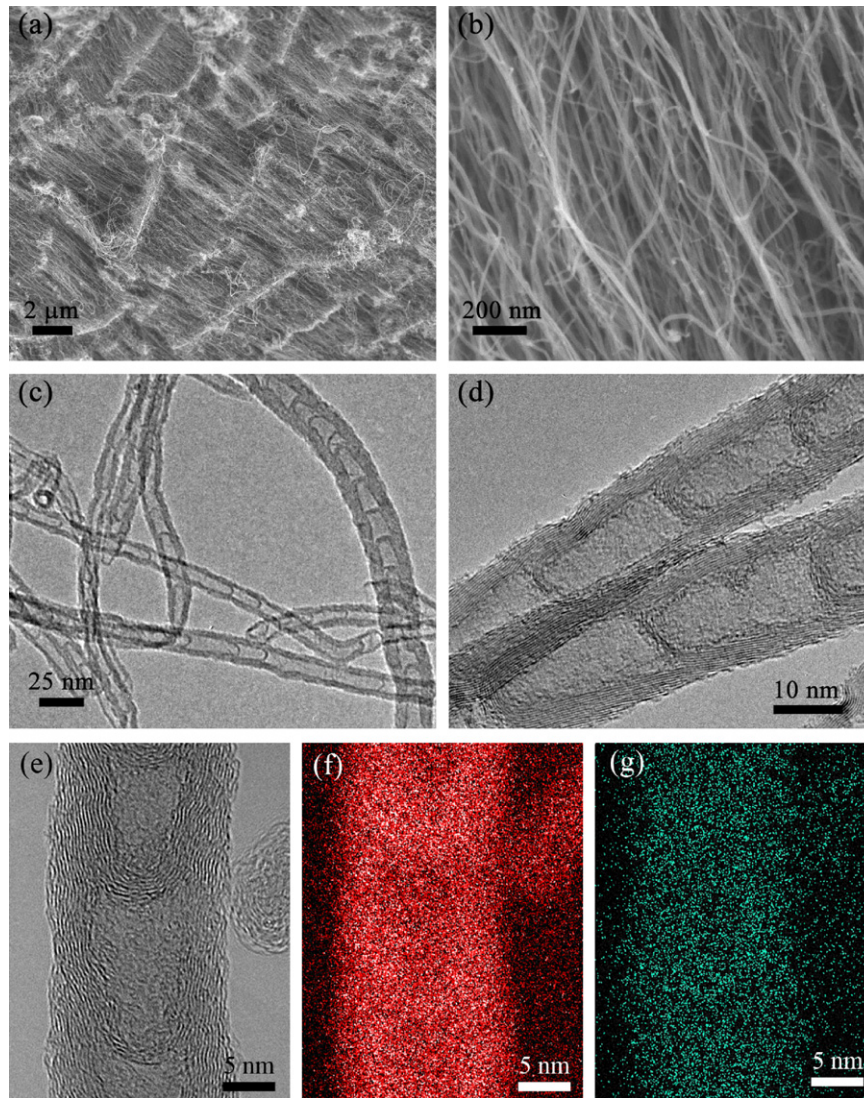


Fig. 10. (a) Low magnification and (b) high magnification SEM images; (c) low magnification and (d) high magnification TEM images of the as-prepared aligned NCNTs with pyridine as nitrogen source at 750 °C; (e) the high resolution TEM and (f–g) the EFTM images of NCNT, where the red color stands for carbon, and the cyanine color stands for nitrogen. (For interpretation of the references to color in this figure legend, the reader is referred to the web version of the article.)

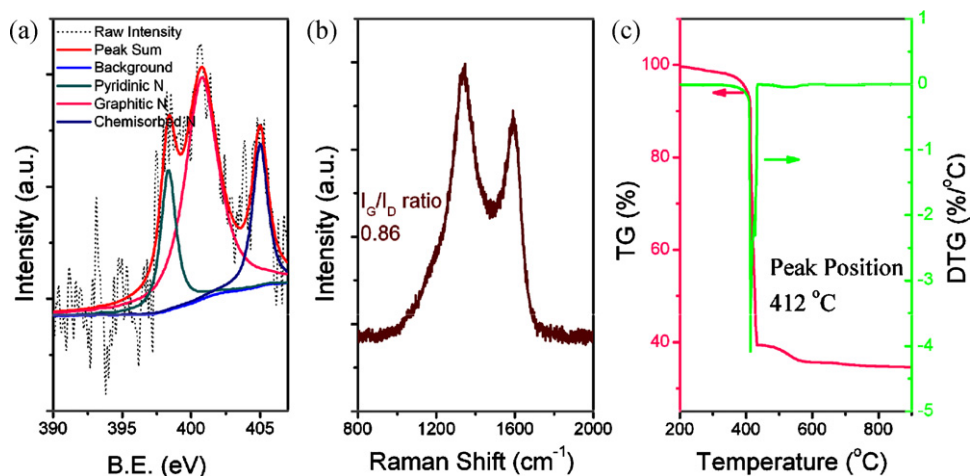


Fig. 11. (a) XPS narrow spectra in N region; (b) Raman spectra; (c) TG and DTG curves for aligned NCNTs with pyridine as nitrogen source at 750 °C.

pyridine often present more complete graphene sheets in contrast with other nitrogen sources like NH_3 [52,55], which may be related with the relatively high C/N ratio of pyridine. In this research, the C/N ratios for NH_3 , 1,2-ethylenediamine, and pyridine were 3.3, 1, and 5, respectively. Higher concentration N may severely affect the precipitation of graphene sheet from catalyst particles and may be responsible for the incomplete graphene sheet structure in the case of NH_3 and 1,2-ethylenediamine. The EFTEM images (Fig. 10e–g) also indicated a uniform distribution of C and N elements. In Fig. 11, XPS revealed that the N content in this sample was 2.45%, mainly composed of graphitic N (62.9%), chemisorbed N oxide (18.3%), and pyridinic N (19.2%). The NCNTs were with similar graphitization degree, and a NCNT yield of $3.75 \text{ g}_{\text{NCNT}}/\text{g}_{\text{cat h}}$ was achieved.

4. Conclusions

Aligned NCNTs were efficiently synthesized in a fluidized bed reactor with NH_3 , 1,2-ethylenediamine, or pyridine as the nitrogen source. The catalyst particles possessed stable fluidization behavior at different growth temperatures during the whole growth process. The aligned NCNTs grew between the catalyst layers and formed a hybrid with alternate aligned CNTs and inorganic layers, which prevented the aligned NCNTs from damage caused by collisions. The CNT bamboo-like structure and N-containing functionalization showed both growth temperature and nitrogen source dependence. The growth temperatures were in the range of 650–800 °C. Generally, higher growth temperature led to a higher NCNT yield (up to $2.95 \text{ g}_{\text{NCNT}}/\text{g}_{\text{cat h}}$ in 800 °C), larger NCNT diameter (about 20 nm), and higher graphitization degree. The change of nitrogen sources also altered the composition of N-containing groups in the CNT products. With the easily scalable fluidization process and the tunable NCNT structures, this work may open a way for the industrial production for such advanced functional material, and promote their applications in electrochemistry, catalysis, energy conversion and storage.

Acknowledgements

The work was supported by the Foundation for the Natural Scientific Foundation of China (Nos. 20736007, 2007AA03Z346), and the China National Program (No. 2011CB932602).

References

- [1] P. Ayala, R. Arenal, M. Rummeli, A. Rubio, T. Pichler, *Carbon* 48 (2010) 575.
- [2] C.P. Ewels, M. Glerup, *J. Nanosci. Nanotechnol.* 5 (2005) 1345.
- [3] K. Xiao, Y.Q. Liu, P.A. Hu, G. Yu, Y.M. Sun, D.B. Zhu, *J. Am. Chem. Soc.* 127 (2005) 8614.
- [4] S.S. Yu, W.T. Zheng, *Nanoscale* 2 (2010) 1069.
- [5] H.Y. Du, C.H. Wang, H.C. Hsu, S.T. Chang, U.S. Chen, S.C. Yen, L.C. Chen, H.C. Shih, K.H. Chen, *Diam. Relat. Mater.* 17 (2008) 535.
- [6] Z. Zhou, X.P. Gao, J. Yan, D.Y. Song, M. Morinaga, *Carbon* 42 (2004) 2677.
- [7] Y.F. Tang, B.L. Allen, D.R. Kauffman, A. Star, *J. Am. Chem. Soc.* 131 (2009) 13200.
- [8] Z. Chen, D. Higgins, Z.W. Chen, *Carbon* 48 (2010) 3057.
- [9] S. van Dommele, K.P. de Jong, J.H. Bitter, *Chem. Commun.* (2006) 4859.
- [10] J. Amadou, K. Chizari, M. Houille, I. Janowska, O. Ersen, D. Begin, C. Pham-Huu, *Catal. Today* 138 (2008) 62.
- [11] F.R. Garcia-Garcia, J. Alvarez-Rodriguez, I. Rodriguez-Ramos, A. Guerrero-Ruiz, *Carbon* 48 (2010) 267.
- [12] J.L. Chen, Z.H. Zhu, S.B. Wang, Q. Ma, V. Rudolph, G.Q. Lu, *Chem. Eng. J.* 156 (2010) 404.
- [13] C. Jin, T.C. Nagaiah, W. Xia, B. Spliethoff, S.S. Wang, M. Bron, W. Schuhmann, M. Muhler, *Nanoscale* 2 (2010) 981.
- [14] H. Liu, Y. Zhang, R.Y. Li, X.L. Sun, S. Desilets, H. Abou-Rachid, M. Jaidann, L.S. Lussier, *Carbon* 48 (2010) 1498.
- [15] K. Chizari, I. Janowska, M. Houille, I. Florea, O. Ersen, T. Romero, P. Bernhardt, M.J. Ledoux, C. Pham-Huu, *Appl. Catal. A* 380 (2010) 72.
- [16] A. Villa, D. Wang, P. Spontoni, R. Arrigo, D.S. Su, L. Prati, *Catal. Today* 157 (2010) 89.
- [17] S. Abate, R. Arrigo, M.E. Schuster, S. Perathoner, G. Centi, A. Villa, D. Su, R. Schlögl, *Catal. Today* 157 (2010) 280.
- [18] R. Chetty, S. Kundu, W. Xia, M. Bron, W. Schuhmann, V. Chirila, W. Brandl, T. Reinecke, M. Muhler, *Electrochim. Acta* 54 (2009) 4208.
- [19] R.T. Lv, T.X. Cui, M.S. Jun, Q. Zhang, A.Y. Cao, D.S. Su, Z.J. Zhang, S.H. Yoon, J. Miyawaki, I. Mochida, F.Y. Kang, *Adv. Funct. Mater.* 21 (2011) 999.
- [20] S.J. Jiang, Y.W. Ma, G.Q. Jian, H.S. Tao, X.Z. Wang, Y.N. Fan, Y.N. Lu, Z. Hu, Y. Chen, *Adv. Mater.* 21 (2009) 4953.
- [21] X. Xu, S.J. Jiang, Z. Hu, S.Q. Liu, *ACS Nano* 4 (2010) 4292.
- [22] D. Hulicova-Jurcakova, M. Kodama, S. Shiraiishi, H. Hatori, Z.H. Zhu, G.Q. Lu, *Adv. Funct. Mater.* 19 (2009) 1800.
- [23] D. Hulicova-Jurcakova, M. Seredych, G.Q. Lu, T.J. Bandosz, *Adv. Funct. Mater.* 19 (2009) 438.
- [24] W.C. Fang, K.H. Chen, L.C. Chen, *Nanotechnology* 18 (2007) 485716.
- [25] D.S. Su, R. Schlögl, *ChemSusChem* 3 (2010) 136.
- [26] K.P. Gong, F. Du, Z.H. Xia, M. Durstock, L.M. Dai, *Science* 323 (2009) 760.
- [27] S.K. Srivastava, V.D. Vankar, D.V.S. Rao, V. Kumar, *Thin Solid Films* 515 (2006) 1851.
- [28] K. Ghosh, M. Kumar, T. Maruyama, Y. Ando, *Carbon* 48 (2010) 191.
- [29] J.H. Bitter, S. Dommele, K.P. de Jong, *Catal. Today* 150 (2010) 61.
- [30] C.V. Rao, C.R. Cabrera, Y. Ishikawa, *J. Phys. Chem. Lett.* 1 (2010) 2622.
- [31] M. Terrones, P.M. Ajayan, F. Banhart, X. Blase, D.L. Carroll, J.C. Charlier, R. Czerw, B. Foley, N. Grobert, R. Kamalakaran, P. Kohler-Redlich, M. Ruhle, T. Seeger, H. Terrones, *Appl. Phys. A* 74 (2002) 355.
- [32] O.Y. Podyacheva, Z.R. Ismagilov, A.E. Shalagina, V.A. Ushakov, A.N. Shmakov, S.V. Tsybulya, V.V. Kriventsov, A.V. Ischenko, *Carbon* 48 (2010) 2792.
- [33] A.E. Shalagina, Z.R. Ismagilov, O.Y. Podyacheva, R.I. Kvon, V.A. Ushakov, *Carbon* 45 (2007) 1808.
- [34] S. van Dommele, A. Romero-Izquierdo, R. Brydson, K.P. de Jong, J.H. Bitter, *Carbon* 46 (2008) 138.
- [35] D.H. Lee, W.J. Lee, S.O. Kim, *Nano Lett.* 9 (2009) 1427.
- [36] M.S. He, S. Zhou, J. Zhang, Z.F. Liu, C. Robinson, *J. Phys. Chem. B* 109 (2005) 9275.
- [37] E.Y. Xu, J.Q. Wei, K.L. Wang, Z. Li, X.C. Gui, Y. Jia, H.W. Zhu, D.H. Wu, *Carbon* 48 (2010) 3097.
- [38] E.N. Nxumalo, P.J. Letsoalo, L.M. Cele, N.J. Coville, *J. Organomet. Chem.* 695 (2010) 2596.
- [39] J. Liu, A.T. Harris, *AIChE J.* 56 (2010) 102.
- [40] Y. Wang, F. Wei, G.H. Luo, H. Yu, G.S. Gu, *Chem. Phys. Lett.* 364 (2002) 568.
- [41] R. Philippe, A. Moranqais, M. Corrias, B. Caussat, Y. Kihn, P. Kalck, D. Plee, P. Gaillard, D. Bernard, P. Serp, *Chem. Vapor Depos.* 13 (2007) 447.
- [42] C.H. See, A.T. Harris, *Ind. Eng. Chem. Res.* 46 (2007) 997.
- [43] F. Wei, Q. Zhang, W.Z. Qian, H. Yu, Y. Wang, G.H. Luo, G.H. Xu, D.Z. Wang, *Powder Technol.* 183 (2008) 10.
- [44] R. Philippe, P. Serp, P. Kalck, Y. Kihn, S. Bordere, D. Plee, P. Gaillard, D. Bernard, B. Caussat, *AIChE J.* 55 (2009) 450.
- [45] Q. Zhang, J.Q. Huang, M.Q. Zhao, W.Z. Qian, F. Wei, *ChemSusChem* 4 (2011) 864.
- [46] Q. Zhang, M.Q. Zhao, Y. Liu, A.Y. Cao, W.Z. Qian, Y.F. Lu, F. Wei, *Adv. Mater.* 21 (2009) 2876.
- [47] Q. Zhang, M.Q. Zhao, J.Q. Huang, Y. Liu, Y. Wang, W.Z. Qian, F. Wei, *Carbon* 47 (2009) 2600.
- [48] Q. Zhang, M.Q. Zhao, J.Q. Huang, J.Q. Nie, F. Wei, *Carbon* 48 (2010) 1196.
- [49] D. Geldart, *Powder Technol.* 7 (1973) 285.
- [50] W.Q. Zheng, J. Zhang, B. Zhu, R. Blume, Y.L. Zhang, K. Schlichte, R. Schlögl, F. Schuth, D.S. Su, *ChemSusChem* 3 (2010) 226.
- [51] H.C. Choi, J. Park, B. Kim, *J. Phys. Chem. B* 109 (2005) 4333.
- [52] J.W. Liu, S. Webster, D.L. Carroll, *J. Phys. Chem. B* 109 (2005) 15769.
- [53] R. Arrigo, M. Havecker, R. Schlögl, D.S. Su, *Chem. Commun.* (2008) 4891.
- [54] R. Arrigo, M. Havecker, S. Wrabetz, R. Blume, M. Lerch, J. McGregor, E.P.J. Parrott, J.A. Zeitler, L.F. Gladden, A. Knop-Gericke, R. Schlögl, D.S. Su, *J. Am. Chem. Soc.* 132 (2010) 9616.
- [55] M. Nath, B.C. Satishkumar, A. Govindaraj, C.P. Vinod, C.N.R. Rao, *Chem. Phys. Lett.* 322 (2000) 333.